Nonlinear forced vibrations of rotating anisotropic beams

Ferhat Bekhoucha, Said Rechak, Laëtitia Duigou, Jean-Marc Cadou

Nonlinear Dynamics manuscript No.
(will be inserted by the editor)

Nonlinear forced vibrations of rotating anisotropic beams

Ferhat Bekhoucha · Said Rechak · Laëtitia Duigou · Jean-Marc Cadou

the date of receipt and acceptance should be inserted later

Abstract This work deals with forced vibration of nonlinear rotating anisotropic beams with uniform cross-sections. Coupling the Galerkin method with the balance harmonic method, the nonlinear intrinsic and geometrically exact equations of motion for anisotropic beams subjected to large displacements, are converted into a static formulation. This latter is treated with two continuation methods. The first one is the asymptotic numerical method, where power series expansions and Padé approximants are used to represent the generalized vector of displacement and the frequency. The second one is the pseudo-arclength continuation method. Numerical tests dealing with isotropic and anisotropic beams are considered. The natural frequencies obtained for prismatic beams are compared with the literature. Response curves are obtained and the nonlinearity is investigated for various geometrical conditions, excitation amplitudes and kinematical conditions. The nonlinearity related to the angular speed for prismatic isotropic beam is thus identified. The stability of the solution branch is examined, in the frequency domain using the Floquet theory.

Keywords Nonlinear vibration of rotating beams · Galerkin method · Harmonic balance method · Asymptotic Numerical Method · Pseudo-arclength

F. Bekhoucha · S. Rechak
Mechanical Engineering and Development Laboratory, Ecole Nationale Polytechnique, Hassen Badi, El Harrach, 16200, Alger, Algeria
E-mail: ferhat.bekhoucha@g.enp.edu.dz

L. Duigou · J. M. Cadou
Laboratoire d'Ingénierie des Matériaux de Bretagne, Université de Bretagne Sud, Rue de Saint Maudé, BP 92116, 56321 Lorient Cedex, France

List of symbols

A	The number of angels per unit area
$\mathcal{A}_{ki}, \bar{\mathcal{A}}$	Matrices used after Galerkin and harmonic balance approximations
B_i	Unit vectors in cross-sectional frame of deformed state
b_i	Unit vectors in cross-sectional frame of undeformed state
e_1	$[1\ 0\ 0]^T$
F	Cross-sectional resultant internal force vector
f	Distributed applied force per unit length vector
H	Cross-sectional angular momentum vector
$\mathbb{i}_2, \mathbb{i}_3, \mathbb{i}_{23}$	Cross-sectional mass moments and product of inertia
$\mathbb{G}, \mathbb{K}, \mathbb{I}$	Component of the Cross-sectional inertia matrix
K	Deformed beam curvature vector
k	Initial curvature vector
L	Length of the beam
M	Cross-sectional internal moment vector
m	Distributed applied moment per unit length vector
P	Cross-sectional linear momentum vector
$\mathbb{R}, \mathbb{S}, \mathbb{T}$	Component of the Cross-sectional flexibility matrix
$\mathbb{U}, \mathbb{V}, \mathbb{W}$	Cross-sectional stiffness matrix components
t	Time
V	Velocity vector of the reference line
x, x_2, x_3	Cross-sectional reference frame of the undeformed beam
$\bar{x}_2, \bar{x}_3$	Offsets from the reference line of the cross-sectional mass center in (b_i)
γ	$[\gamma_{11}\ 2\gamma_{12}\ 2\gamma_{13}]^T$
Δ	Identity matrix

$\kappa_1, \kappa_2, \kappa_3$	Twist and bending curvatures ($\kappa_i = K_i - k_i$)
μ	Mass per unit length
ρ	Mass density
Ω	Angular velocity vector
$(\bullet')$	$\partial(\bullet)/\partial x_1$
$(\dot{\bullet})$	$\partial(\bullet)/\partial t$
$(\tilde{\bullet})$	$-e_{ijk}(\bullet)_k$
ANM	Asymptotic Numerical Method
PAL	Pseudo-arclength method

1 Introduction

Many studies have been performed for modeling the rotating flexible beams. The earlier linear analytical model to calculate the natural frequencies, based on the Rayleigh energy theorem, is attributed to Southwell and Gough [1] and has been extended by many studies based on different analytical methods, Putter and Manor [2], Wright et al. [3]. Later, complex models were developed to obtain accurate natural frequencies, introducing effects, such as the cross-sectional variation, Klein [4], and the pretwist Swaminathan and Rao [5]. Recently, other models have been developed for the vibration analysis of Timoshenko beams, including effects such as non-uniformity, pretwist and offset root [6,7,9]. In these models, the nonlinear terms are truncated and thus are valid for only linear vibration.

A number of geometrically exact formulations for the nonlinear dynamics of beams were developed, that can be used for nonlinear vibrations of beams; Borri and Mantegazza 1985 [10] Bauchau and Kang 1993 [11]. Gemetrically exact means that there is no approximation made to the geometrie of the large deformation which concerne the deformed beam reference line and the orientation of the cross-section frame. These theories are displacement-based formulations; the governing equations must contain displacements and finite rotations variables and the solution needs at the most a finite-element method (FEM) formulation against a large number of variables.

The present study is based on the intrinsic formulation developed by Hodges [12, 13]. This formulation covers a beam undergoing large deformation and small strain. It takes advantage of the one dimensional characteristic of a beam, does not require definitions for displacement and rotation variables and it is less expensive than using three dimensional (3D) finite-element meth- od (FEM). A Galerkin approach is applied to this model, where the weighting functions are chosen to be the assumed modes themselves. This leads to an energy balance and consequently, provides a better numerical approximation of the solution of the nonlinear beam equations [14–16]. Using this discretization and the harmonic balance method, the set of initial differential equations are reduced to one algebraic equation, where the beam is subjected to harmonic excitation at the tip.

The Asymptotic Numerical Method (ANM) which uses power series expansion of the unknowns associated with Padé approximants [17, 18], and the pseudo-arclength method (PAL) [28] are used to provide dynamic response of the excited beam. The ANM has been successfully applied to solve nonlinear problems, such as nonlinear elasticity [17], nonlinear vibrations [19–21] or in fluid mechanics [22], it is often introduced in the elementary step of discretization using FEM [17–23]. In our study, these two continuation methods are introduced after a discretization with a Galerkin approach and harmonic balance methods leading to an algebraic equation.

The aim of this paper is to explore the nonlinearities of the isotropic prismatic beams excited harmonically, associated with various conditions: initial pretwist, uniform angular speed and offset root. Furthermore, a composite beam that presents a nonhomogenous material is examined. The numerical examples presented deal with cases already treated in the literature, in the manner of a classical linear study. The stability of the solution is studied by using the Floquet exponents.

2 Mathematical formulation

2.1 Nonlinear intrinsic equations

Based on a Timoshenko beam model, the Euler-Lagrange nonlinear equations of motion derived from Hamilton's principle are [12]:

$$F' + (\tilde{\mathbb{k}} + \tilde{\kappa})F + f = \dot{P} + \tilde{\Omega}P \quad (1)$$

$$M' + (\tilde{k} + \tilde{\kappa})M + (\tilde{e_1} + \tilde{\gamma})F + m = \dot{H} + \tilde{\Omega}H + \tilde{V}P \quad (2)$$

where, as mentioned in the nomenclature, $(')$ denotes the derivative with respect to the undeformed beam reference line defined by the curvilinear coordinate x as illustrated in Fig. 1, $(\dot{})$ denotes the absolute time derivative and $(\tilde{v})$ is the antisymmetric matrix associated with a vector $v = [v_1 \ v_2 \ v_3]^T$. A local coordinate system $(b_i(x), i = 1, 2, 3)$, is defined on each point (i.e. cross-section), along the undeformed reference line, which transforms into a deformed frame $B_i(x)$. A global

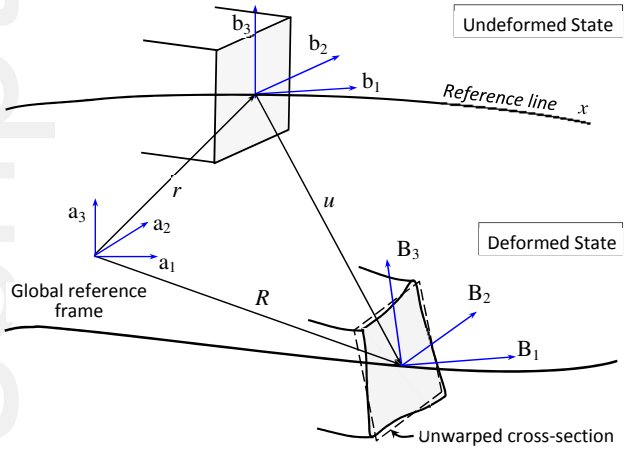

Fig. 1 Schematic of beam model, frames and reference line

reference frame $a_i(x)$ is also defined, used for the discription of displacement fields.

F is the internal force vector, composed of an axial force and two shear forces; M is the internal moment, composed of a twisting moment and two bending moments. They are related to generalized strains γ and ($\kappa = K - \mathbb{k}$), with the assumption of small strain, by the constitutive equation,

$$\begin{Bmatrix} F \\ M \end{Bmatrix} = \begin{pmatrix} \mathbb{U} & \mathbb{V} \\ \mathbb{V}^T & \mathbb{W} \end{pmatrix} \begin{Bmatrix} \gamma \\ \kappa \end{Bmatrix} = \boldsymbol{S} \begin{Bmatrix} \gamma \\ \kappa \end{Bmatrix} \tag{3}$$

In Eqs. (1) and (2), P and H are the linear and angular momentums vectors, related to V and Ω, the linear and angular velocities vectors by the equation,

$$\begin{Bmatrix} P \\ H \end{Bmatrix} = \begin{pmatrix} \mu\Delta & -\mu\tilde{\bar{x}} \\ \mu\tilde{\bar{x}} & \mathbb{I} \end{pmatrix} \begin{Bmatrix} V \\ \Omega \end{Bmatrix} = \begin{pmatrix} \mathbb{G} & \mathbb{K} \\ \mathbb{K}^T & \mathbb{I} \end{pmatrix} \begin{Bmatrix} V \\ \Omega \end{Bmatrix} \tag{4}$$

where μ is the mass per unit length, $\tilde{\bar{x}}$ is the antisymmetric matrix associated with $\bar{x} = [0\ \bar{x}_2\ \bar{x}_3]^T$, the offset from the reference line of the cross-sectional mass center, and $\mathbb{I}$ is composed of cross-sectional mass moments and the product of inertia as,

$$\mathbb{I} = \begin{bmatrix} \mathbb{i}_2 + \mathbb{i}_3 & 0 & 0 \\ 0 & \mathbb{i}_2 & \mathbb{i}_{23} \\ 0 & \mathbb{i}_{23} & \mathbb{i}_3 \end{bmatrix} \tag{5}$$

where $\mathbb{U}$, $\mathbb{V}$ and $\mathbb{W}$ are matrices (3×3) and represent the components of the stiffness matrix $\boldsymbol{S}(6 \times 6)$, γ and κ are the generalized strains (beam strains and curvatures) and k is the initial curvature vector. For prismatic isotropic beams, the stiffness matrix S is diagonal and can be calculated in closed form, in which the reference line is chosen to be the one formed by the locus of the cross-sectional centroids and the centroidal axis are along x_2 and x_3. But, for complex cross section and anisotropic beams, a 2-D FEM analysis is required to determine the stiffness matrix S, as in [24], in which the results are obtained by using VABS code based on the variational asymptotic method (VAM) developed by Berdichevsky (1976) [24,25]. Moreover, the stiffness matrix for prismatic and isotropic beams with an initial curvature is not diagonal i.e. the component $\mathbb{V}$ is not zero.

The nonlinear intrinsic equations of motion of a beam, Eqs. (1) and (2), are solved along with two other nonlinear kinematical equations [13]:

$$V' + (\tilde{\mathbb{k}} + \tilde{\kappa})V + (\tilde{e_1} + \tilde{\gamma})\Omega = \dot{\gamma} \tag{6}$$

$$\Omega' + (\tilde{\mathbb{k}} + \tilde{\kappa})\Omega = \dot{\kappa} \tag{7}$$

The partial differential equations (1), (2), (6) and (7) with the algebraic equations (3) and (4) represent the system of nonlinear intrinsic equations for the dynamics of a general beam undergoing small local strains and large deformations. The associated boundary conditions for a given fixed-free beam with a length L are:

$$\begin{cases} x = 0, (\text{fixed end}) : V(0,t) = V^0, \quad \Omega(0,t) = \Omega^0 \\ x = L, (\text{free end}) \ : F(L,t) = F^L, \ M(L,t) = M^L \end{cases} \tag{8}$$

To solve the above system in the frequency domain with these boundary conditions, the Galerkin approximation will be used to transform this system to one differential equation, after which it will be converted to one algebraic equation by using the harmonic balance method.

2.2 Energy-consitent weighting

Consider the following weighting of all governing equations (1) , (2), (6) and (7) as well as the boundary conditions (8) :

$$\int_0^L \Big\{ V^T\Big[\dot{P} + \tilde{\Omega}P - F' - (\tilde{k}+\tilde{\kappa})F - f\Big] + \Omega^T\Big[\dot{H} + \tilde{\Omega}H + \tilde{V}P - M' - (\tilde{k}+\tilde{\kappa})M - (\tilde{e_1}+\tilde{\gamma})F - m\Big] + F^T\Big[\dot{\gamma} - V' - (\tilde{k}+\tilde{\kappa})V - (\tilde{e_1}+\tilde{\gamma})\Omega\Big] + M^T\Big[\dot{\kappa} - \Omega' - (\tilde{k}+\tilde{\kappa})\Omega\Big] \Big\} dx - F^T(0,t)\Big[V(0,t) - V^0\Big] - M^T(0,t)\Big[\Omega(0,t) - \Omega^0\Big] + V^T(L,t)\Big[F(L,t) - F^L\Big] + \Omega^T(L,t)\Big[M(L,t) - M^L\Big] = 0 \quad (9)$$

After integrating by parts of terms $V^T F'$ and $M^T \Omega'$ and simplifying Eq.(9), we obtain:

$$\int_0^L \Big[V^T\dot{P} + \Omega^T\dot{H}\Big]dx + \int_0^L \Big[F^T\dot{\omega} + M^T\dot{\kappa}\Big]dx = \int_0^L \Big[V^T f + \Omega^T m\Big]dx + \Big[V^T(L,t)F^L + \Omega^T(L,t)M^L - F^T(0,t)V^0 - M^T(0,t)\Omega^0\Big] \quad (10)$$

where the left terms of this equality are the rates of change of kinetic energy and potential energy respectively, and the right terms are the rates of works due to the external forces in the interior of the beam and the applied forces at the boundaries. This stipulates the energy conservation and motivates the use of Eq.(9) to derive a Galerkin approach to solve the governing partial differential equations, in which the weighting functions were also used as the trial functions.

2.3 Galerkin approximation

Using the shifted Legendre polynomials as trial functions, the primary variables $V(x,t)$, $\Omega(x,t)$, $F(x,t)$ and $M(x,t)$ are approximated as follows:

$$\begin{aligned} V(x,t) &= \sum_{i=1}^{nf} \Phi_i(x) v_i(t), \quad \Omega(x,t) = \sum_{i=1}^{nf} \Phi_i(x)\bar{\omega}_i(t) \\ F(x,t) &= \sum_{i=1}^{nf} \Phi_i(x) f_i(t), \quad M(x,t) = \sum_{i=1}^{nf} \Phi_i(x) m_i(t) \end{aligned} \quad (11)$$

where $(nf\ )$ is the number of trial functions used, $v_i(t)$, $\bar{\omega}_i(t)$, $f_i(t)$ and $m_i(t)$ are three component vectors and,

$$\Phi_i(x) = \begin{bmatrix} \mathcal{P}_{i-1}(x) & 0 & 0 \\ 0 & \mathcal{P}_{i-1}(x) & 0 \\ 0 & 0 & \mathcal{P}_{i-1}(x) \end{bmatrix} \quad (12)$$

where $\mathcal{P}_i(x)$ are the shifted Legendre functions [26] used as trial functions. $P(x,t)$, $H(x,t)$, $\gamma(x,t)$ and $\kappa(x,t)$ are the secondary variables, related to the primary variable by the constitutive equations (3) and (4).

A new generalized vector (q) is defined:

$$q = [q_1\ q_2 \cdots q_{nf}]^T \quad \text{with} \quad q_i = [v_i(t)\ \bar{\omega}_i(t)\ f_i(t)\ m_i(t)]^T \quad (13)$$

With the assumption of a constant cross-section, constant curvature and constant distributed bending, Eq.(9) is transformed into one differential equation in time as [16]:

$$\mathcal{A}_{ki}\dot{q} + \mathcal{B}_{ki}q + \mathcal{C}_{kij}q.q + \mathcal{D}_k + f_k + m_k = 0 \quad (14)$$

where the coefficient of the nonlinear term, matrix $\mathcal{C}_{kij}$, is function only of stiffness and mass matrices of the beam's cross-section [15].

The natural frequencies are obtained from a linearization of Eq.(14) around a steady state solution ($\dot{q} = 0, q = q_0$), with no distributed force and moment ($f_k = 0$, $m_k = 0$), and inserting a solution $q = Xe^{\omega t}$ [14].

$$\hat{\mathcal{A}}_{ki}\dot{q} + \hat{\mathcal{B}}_{ki}q = 0 \quad (15)$$

where X is the eigenvector, ω is the natural frequency and

$$\hat{\mathcal{A}}_{ki} = \mathcal{A}_{ki} \quad \text{and} \quad \hat{\mathcal{B}}_{ki} = \mathcal{B}_{ki} + (\mathcal{C}_{kij} + \mathcal{C}_{kji})q_0 \quad (16)$$

2.4 Harmonic balance method

In the following, a fixed-free beam harmonically excited at the tip is considered. No distributed forces or moments are present. The excitation force $F^L(t)$ is computed in the vector $\mathcal{D}_k$, thus Eq.(14) is reduced to:

$$\mathcal{A}_{ki}\dot{q} + \mathcal{B}_{ki}q + \mathcal{C}_{kij}q.q + \mathcal{D}_k = 0 \quad (17)$$

The harmonic excitation is given by:

$$F^L(t) = F_0 cos\omega t \quad (18)$$

It is assumed that the response of the beam is harmonic and can be given as follows:

$$q(t) = \sum_{j=0}^{H-1} (q_j^c cos j\omega t + q_j^s sin j\omega t) \quad (19)$$

New vector ($\bar{q}$) is introduced, containing all the harmonics and defined by:

$$\bar{q} = [q_0^{cT}\ q_1^{cT}\ q_1^{sT} \cdots q_j^{cT}\ q_j^{sT} \cdots q_{H-1}^{c\ T}\ q_{H-1}^{s\ T}]^T \quad (20)$$

By inserting series Eq.(19) and using the harmonic balance method, the governing equation (17) is rewritten in the frequency domain as:

$$\mathcal{F}(\bar{q}, \omega) = \omega \bar{\mathcal{A}} \bar{q} + \bar{\mathcal{B}} \bar{q} + \bar{\mathcal{C}} \bar{q}.\bar{q} + \bar{\mathcal{D}} = 0 \quad (21)$$

where matrices $\bar{\mathcal{A}}, \bar{\mathcal{B}}, \bar{\mathcal{C}}$ and $\bar{\mathcal{D}}$ are derived from matrices $\mathcal{A}_{ki}$, $\mathcal{B}_{ki}$, $\mathcal{C}_{kij}$ et $\mathcal{D}_k$. For example, for three harmonics,

$$q(t) = q_0^c + q_1^c cos\omega t + q_1^s sin\omega t + q_2^c cos2\omega t + q_2^s sin2\omega t \quad (22)$$

In matrix format:

$$\bar{q} = [q_0^{cT}\ q_1^{cT}\ q_1^{sT}\ q_2^{cT}\ q_2^{sT}]^T \quad (23)$$

The product $\mathcal{B}_{ki} q$ is rewritten as:

$$\mathcal{B}_{ki} q \equiv \bar{\mathcal{B}} \bar{q} = \begin{bmatrix} \mathcal{B}_{ki} & 0 & 0 & 0 & 0 \\ 0 & \mathcal{B}_{ki} & 0 & 0 & 0 \\ 0 & 0 & \mathcal{B}_{ki} & 0 & 0 \\ 0 & 0 & 0 & \mathcal{B}_{ki} & 0 \\ 0 & 0 & 0 & 0 & \mathcal{B}_{ki} \end{bmatrix} . \begin{bmatrix} qc_0 \\ qc_1 \\ qs_1 \\ qc_2 \\ qs_2 \end{bmatrix} \quad (24)$$

$\bar{\mathcal{A}}$ is obtained after derivation of Eq.(22) with respect to time, where the first term is constant and has a null derivative, the product $\mathcal{A}_{ki}\dot{q}$ will have another disposition that:

$$\bar{\mathcal{A}} = \begin{bmatrix} 0 & 0 & 0 & 0 & 0 \\ 0 & 0 & \mathcal{A}_{ki} & 0 & 0 \\ 0 & -\mathcal{A}_{ki} & 0 & 0 & 0 \\ 0 & 0 & 0 & 0 & 2\mathcal{A}_{ki} \\ 0 & 0 & 0 & -2\mathcal{A}_{ki} & 0 \end{bmatrix} \quad (25)$$

Because $\mathcal{C}_{kij} q.q$ is quadratic, one has to determine first the matrix representation of $\bar{\mathcal{C}}\bar{q}$, that can be obtained by a harmonic balance of the product of two vectors with the same order of harmonics:

$$\bar{\mathcal{C}}\bar{q} = \begin{bmatrix} \mathcal{C}_{kij}(q_0^c)\ \mathcal{C}_{kij}(\frac{q_1^c}{2}) & \mathcal{C}_{kij}(\frac{q_1^s}{2}) & \mathcal{C}_{kij}(\frac{q_2^c}{2}) & \mathcal{C}_{kij}(\frac{q_2^s}{2}) \\ \mathcal{C}_{kij}(q_1^c)\ \mathcal{C}_{kij}(q_0^c + \frac{q_2^c}{2}) & \mathcal{C}_{kij}(\frac{q_2^s}{2}) & \mathcal{C}_{kij}(\frac{q_1^c}{2}) & \mathcal{C}_{kij}(\frac{q_1^s}{2}) \\ \mathcal{C}_{kij}(q_1^s)\ \mathcal{C}_{kij}(\frac{q_2^s}{2}) & \mathcal{C}_{kij}(q_0^c - \frac{q_2^c}{2}) & \mathcal{C}_{kij}(-\frac{q_1^s}{2}) & \mathcal{C}_{kij}(\frac{q_1^c}{2}) \\ \mathcal{C}_{kij}(q_2^c)\ \mathcal{C}_{kij}(\frac{q_1^c}{2}) & \mathcal{C}_{kij}(-\frac{q_1^s}{2}) & \mathcal{C}_{kij}(q_0^c) & 0 \\ \mathcal{C}_{kij}(q_2^s)\ \mathcal{C}_{kij}(\frac{q_1^s}{2}) & \mathcal{C}_{kij}(\frac{q_1^c}{2}) & 0 & \mathcal{C}_{kij}(q_0^c) \end{bmatrix} \quad (26)$$

The first component of vector $\bar{\mathcal{D}}$ concerns the constant part of $\mathcal{D}_k$ given by the boundary conditions. The second component deals with the amplitude F_0 of the harmonic excitation $F^L(t) = F_0 cos\omega t$, and the rest of the components are zeros. Our objective is to solve equation (21), which is quadratic with respect to $\bar{q}$ and has a parameter ω, with a continuation method. In this paper, we use both the asymptotic numerical method and pseudo-arclength method.

2.5 Asymptotic numerical method

In this section, an algorithm based on the asymptotic numerical method (ANM) is developed to solve the forced vibration problem Eq.(21) and obtain the response curves. The ANM has been successfully used to study many nonlinear problems [17, 19–21].
The unknowns in Eq.(21) are the vector $\bar{q}$ and the frequency ω that can be developed in a power series with respect to path parameter 'a' in the vicinity of a regular solution $(\bar{q}_0, \omega_0)$, which is known except for the first step of the computation:

$$\begin{cases} \bar{q}(a) = \bar{q}_0 + \sum_{j=1}^{n} a^j \bar{q}_j \\ \omega(a) = \omega_0 + \sum_{j=1}^{n} a^j \omega_j \end{cases} \quad (27)$$

in which $\bar{q}_j$ and ω_j are the new unknowns which have to be computed. The path parameter 'a' can be defined as the projection of the increments of $\bar{q}$ and ω on the tangent vector $(\bar{q}_1, \quad \omega_1)$:

$$a = (\bar{q} - \bar{q}_0)^T \bar{q}_1 + (\omega - \omega_0)\omega_1 \quad (28)$$

Introducing the polynomial developements Eqs.(27) into Eqs.(21) and (28) and equating like powers of 'a', one obtains the following set of linear systems except the zeroth order is nonlinear:

Order 0

$$\mathcal{F}(\bar{q}_0, \omega_0) = \omega \bar{\mathcal{A}} \bar{q}_0 + \bar{\mathcal{B}} \bar{q}_0 + \bar{\mathcal{C}} \bar{q}_0.\bar{q}_0 + \bar{\mathcal{D}} = 0 \quad (29)$$

The zeroth order is related to the first point of the branch. Generally ω_0 is taken zero, thus $\bar{q}_0$ corresponds to the steady state solution and can be obtained by a Newton-Raphson method. This is only carried out for

the initial step of the continuation method

Order 1

$$\begin{cases} \mathcal{F}_{\bar{q}}\ \bar{q}_1 \ = \ -\omega_1 \bar{\mathcal{A}} \bar{q}_0 \\ \bar{q}_1^T . \bar{q}_1 \ + \ \omega_1^2 = 1 \end{cases} \tag{30}$$

Order p

$$\begin{cases} \mathcal{F}_{\bar{q}}\ \bar{q}_p \ = \ D_p \\ \bar{q}_1^T . \bar{q}_p + \omega_1 \omega_p \ = \ 0 \end{cases} \tag{31}$$

$$\text{with} \quad D_p = -\omega_p \bar{\mathcal{A}} \bar{q}_0 - \sum_{i=1}^{p-i} \omega_{p-1} \bar{\mathcal{A}} \bar{q}_i + \bar{\mathcal{C}} \bar{q}_i . \bar{q}_{p-i}$$

where the Jacobian, considered regular at $\bar{q}_0$, is defined by:

$$\mathcal{F}_{\bar{q}} = \omega_0 \bar{\mathcal{A}} + \bar{\mathcal{B}} + 2\bar{\mathcal{C}} \bar{q}_0 \tag{32}$$

The polynomial solutions Eq.(27) agree well in the zone of validity [0 a_{ms}] and diverge out of this zone. The limit a_{ms} can be computed automatically using a simple criterion proposed in [18]:

$$a_{ms} = \left(\eta_s \frac{\|\bar{q}_1\|}{\|\bar{q}_n\|} \right)^{1/(n-1)} \tag{33}$$

where η_s is a small given parameter.

This algorithm can be improved by replacing the polynomial representation Eq.(27) by rational fractions named Padé approximants [17]:

$$\begin{cases} \bar{q}_n(a) = \ \bar{q}_0 + \sum_{j=1}^{n-1} f_j(a) a^j \bar{q}_j \\ \omega_n(a) = \omega_0 + \sum_{j=1}^{n-1} f_j(a) a^j \omega_j \end{cases} \tag{34}$$

in which $f_j(a)$ are rational fractions with the same denominator. The zone of validity of this rational representation [0 a_{mp}] is defined by the maximal value of 'a' that can verify the condition [17]:

$$\frac{\|\bar{q}_n(a_{mp}) - \bar{q}_{n-1}(a_{mp})\|}{\|\bar{q}_n(a_{mp}) - \bar{q}_0\|} \leqslant \eta_s \tag{35}$$

i.e., the relative difference between the displacements at two consecutive orders must be smaller than a given number η_p .at the end of the step

Iteratively reapplying this algorithm by taking a new starting point in the zone of validity of the brevious step makes it possible to determine the entire of the response curve.

2.6 Pseudo arc-length method

Another algorithm based on the pseudo-arclength method (PAL) [28] is presented in order to validate the obtained results. This method is a predictor-corrector's scheme and is based on two steps:

Step 1: Prediction

The differentiation of Eq.(21) with respect to the path parameter at $(\bar{q}_0, \omega_0)$ yields:

$$\mathcal{F}_{\bar{q}} \bar{q}_0' + \mathcal{F}_\omega {\omega_0}' = 0 \tag{36}$$

where $\mathcal{F}_{\bar{q}}$ is defined in Eq.(29) and

$$\mathcal{F}_\omega = \frac{\partial \mathcal{F}}{\partial \omega} = \bar{\mathcal{A}} \bar{q} \tag{37}$$

For a normalized tangent vector $({\bar{q}_0'}^T . \bar{q}_0' + {\omega_0'}^2 = 1)$ yields:

$$\omega_0' = \pm (1 + z^T . z)^{-1/2} \tag{38}$$

where from Eq.(36),

$$\bar{q}_0' = \omega_0' z \text{ , with } z = -\mathcal{F}_{\bar{q}}^{-1} \mathcal{F}_\omega \tag{39}$$

The sign in Eq.(36) determines the direction of continuation. Thus, the predicted point is defined by:

$$\begin{cases} \bar{q}_1 = \ \bar{q}_0 + \bar{q}_0' \ \Delta s \\ \omega_1 = \omega_0 + {\omega_0}' \Delta s \end{cases} \tag{40}$$

Step 2: Correction

This point is corrected along the normal of the tangent vector $({\bar{q}_0'}^T, \omega_0')^T$. One gets another equation:

$$\boldsymbol{G}(\bar{q}, \omega) = (\bar{q} - \bar{q}_0)^T \bar{q}_0' + (\omega - \omega_0) \omega_0' - \Delta s = 0 \tag{41}$$

Eqs.(21) and (41) define the nonlinear system to be solved by the Newton method. The unknowns at the iteration $(k+1)$ are defined by:

$$\begin{cases} \bar{q}_{k+1} = \ \bar{q}_k + \Delta \bar{q} \\ \omega_{k+1} = \omega_k + \Delta \omega \end{cases} \tag{42}$$

By introducing these two increments into the nonlinear Eqs. (21) and (41) and by neglecting second order terms in $\Delta \bar{q}$ and $\Delta \omega$, one obtains the following linear system to be solved at each Newton iteration:

$$\begin{cases} \mathcal{F}_{\bar{q}} \Delta \bar{q} + \mathcal{F}_\omega \Delta \omega = -\mathcal{F}(\bar{q}, \omega) \\ {\bar{q}'}^T \Delta \bar{q} + \omega' \Delta \omega \ = -\boldsymbol{G}(\bar{q}, \ \omega) \end{cases} \tag{43}$$

2.7 Stability of the solutions

The study of the local stability is crucial to state within the obtained solution, if it is physically feasible or not. This stability is studied by adding a small disturbance to a considered solution q_0 at ω_0:

$$q(t) = q_0(t) + Q(t) \tag{44}$$

The stability of q_0 is related to the behavior of the disturbance Q. If this disturbance disappears with time, then q_0 is stable, if it increases then q_0 is unstable. This disturbance is first studied in the time domain and then by applying the HBM, we return to the frequency domain, which will be suitable for both continuation methods ANM and pseudo-arclength. Substituting Eq. (44) into Eq. (17), expanding the result in a Taylor series in the vicinity of q_0 and keeping only the linear terms in the disturbance, one obtains:

$$\mathcal{A}_{ki}\dot{Q} + \mathcal{B}_{ki}Q + 2\mathcal{C}_{kij}q_0.Q = 0 \tag{45}$$

Using the Floquet form, the disturbance can be expressed as a product of periodic and exponent components

$$Q(t) = e^{\mu t}\sum_{j=0}^{\bar{H}-1}(Q_j^c cos j\omega t + Q_j^s sin j\omega t) \tag{46}$$

where μ are the Floquet exponents to be determined. Inserting Eq. (46) into Eq. (45) and using the HBM, the following eigenvalue problem is obtained

$$\Big\{(-\bar{M}\bar{K}) - \mu I\Big\}\bar{Q} = 0 \tag{47}$$

where, $\bar{Q} = [Q_0^{c\,T}\ Q_1^{c\,T}\ Q_1^{s\,T}...\ Q_{\bar{H}-1}^{c\,T}\ Q_{\bar{H}-1}^{s\,T}]^T$, I is the identity matrix, $\bar{H}$ is the number of harmonics used in the study of stability. As stated in [35], it can be different from the number of harmonics H used in the continuation step,

$$\bar{K} = \omega_0\bar{\mathcal{A}} + \bar{\mathcal{B}} + 2\bar{\mathcal{C}}\bar{q}_0 \tag{48}$$

and for $\bar{H} = 3$,

$$\bar{M} = \begin{bmatrix} \mathcal{A}_{ki} & 0 & 0 & 0 & 0 \\ 0 & \mathcal{A}_{ki} & 0 & 0 & 0 \\ 0 & 0 & \mathcal{A}_{ki} & 0 & 0 \\ 0 & 0 & 0 & \mathcal{A}_{ki} & 0 \\ 0 & 0 & 0 & 0 & \mathcal{A}_{ki} \end{bmatrix}. \tag{49}$$

The number of Floquet exponents necessary to determine the stability of the solution is $(12\ n_f)$ and will be selected among all the eigenvalues of the system Eq. (47). We adopt the method of selection used in [36], based on the comparison of median eigenvectors.

By definition, if x_j is the j^{th} component of a vector x, the median is $\sum_j j|x_j|/\sum_j |x_j|$.

The eigenvalues selected correspond to the eigenvectors having medians closest to the value $[12\ n_f(2\bar{H}-1)]/2$. These Floquet exponents $\mu_i, i = 1, ...12\ n_f$ are used to states on the stability of the solution.

If $\Re(\mu_i) < 0$ for all i, the solution is asymptotically stable. If $\Re(\mu_i) > 0$ for any $i = 1, ...12\ n_f$, the solution is unstable.

2.8 Dimensionless parameters

To be able to compare with results in the literature, several dimensionless parameters are introduced [6, 7]:

$$\begin{aligned} &\Omega^* = \Omega_3 T, \quad \omega^* = \omega T, \quad T = \sqrt{\frac{\mu L^4}{EI_2}} \\ &\delta_h = \frac{r}{L}, \qquad \delta_I = \frac{I_2}{I_3}, \quad \beta = \sqrt{\frac{AL^2}{I_2}} \end{aligned} \tag{50}$$

where, r is the rayon of the hub, μ is the mass per unit length, I_2 and I_3 are the second area moments of inertia of the cross-section about the x_2 and x_3 axes respectively. The variables Ω^* , ω^*, δ_h, δ_I and β represent the angular speed ratio, the frequency ratio, the hub radius ratio, the second area moments of inertia ratio and the slenderness ratio, respectively.

3 Numerical results

In this part, numerical simulations for forced vibrations of fixed-free uniform isotropic and anisotropic beams were performed. Various conditions which concern the angular speed of the fixed end, the hub radius are taken in the analysis. The codes used for the calculus of the natural frequencies and branches of continuations are implemented using the Matlab environment, whereas the cross-sectional properties of the particular beams studied herein are obtained from the literature [6, 15, 16, 24, 31]. Based on previous studies, the number of assumed modes in Galerkin approximation is taken $n_f = 10$, shown optimal and used for all cases presented in [14]. The number of harmonics $H = 3$ is adopted for an optimal computational time [21, 23] and $\bar{H} = 6$ for the stability study [35]. The adopted parameters for ANM

are: the truncation order $n = 15$ [22], the accuracy parameter is taken $\eta_s = 10^{-4}$ for series-continuation and $\eta_p = 10^{-4}$ for Padé-continuation [20, 21], against accuracy parameters $\epsilon = 10^{-7}$ for the Newton-Raphson method. For the PAL continuation method the step is taken $\Delta s = 1.5$ in order to obtain a smooth curve.

3.1 Isotropic beam

At first, it is important to validate this approach for classical beams before dealing with composite beams. Homogenous, isotropic and prismatic beams are examined in free and forced vibration. Table 1 shows the variation of the first and second chordwise bending natural frequencies of uniform beam with respect to the slenderness ratio β and the dimensionless angular speed Ω^*. The natural frequencies are obtained from Eq.(15), using the Matlab function (`eig`) applied to matrices of size (120 x 120). The results obtained from the present approach show a perfect coherence with the references [6,7], in both cases of Euler-Bernoulli beam (EB), corresponding to ($\beta \geqslant 1000$) and Timoshenko beam without angular speed. For a Timoshenko beam ($\beta = 50 \div 10$) with a non-zero angular speed, frequencies obtained are smaller than those of [6, 7] with significant differences. The reason is that the energy expressions used in these works are approximated while the one used in this approach is without approximation since the equations of motion and the kinematical equations are exact. Similar results were obtained in [8], where the shear and rotary inertia effects are neglected. In this work, it is concluded that the gyroscopic coupling between the stretching and bending motions significantly decreases the natural frequencies and that this coupling effect becomes negligible as the slenderness ratio of the beam increases.

Indeed, in [7], the governing equations of motion are derived using Lagrange's equations from the kinetic and potential energy expressions which are obtained from a set of hybrid deformation variables. These equations are simplified by neglecting the gyroscopic coupling between stretching and bending. A similar simplification is explained in [30]. These coupling terms do not appear in the equations of motion derived in [6], using the Hamilton's principle, where the kinetic and potential energies are based on a truncation scheme. The latter kind of theory is addressed in [25], Chapter 1. Hence, the natural frequencies obtained in [6] and [7] are relatively close.

Table 2 shows the four lowest non-dimensional natural frequencies of a pretwisted non-rotating Euler-Bernoulli beam for different values of the total angle of pre-twist (α). It can be observed that there is a perfect accordance between the present results and those given in [9, 30]. In order to compare results with the literature, these non-dimensional frequencies are calculated using I_3 instead of I_2 in Eq.(50). The values corresponding to the second and the fourth modes are close to those in Table 1. In both studies [9,30], the potential energy expressions are derived from a set of hybrid deformation variables and the coupling effect between the stretching and the bending motions is ignored. It is also observed that the non-zero terms submerged in $\mathbb{V}$, component of the stiffness matrix $\boldsymbol{S}$, have less influence on the natural frequencies.

Table 2
Comparison of the four lowest natural frequencies for a non-rotating beam according to the angle of pre-twist α, ($\beta = 1000, \gamma = 0, \delta_h = 0, \delta_I = 0.25, k_sG/E = 0.25$)

	α^o	Present	[30]	[9]
1^{rst}				
	30	1.7623	1.7622	1.7623
	60	1.7748	1.7748	1.7748
	90	1.7950	1.7950	1.7950
2^{nd}				
	30	3.4793	3.4793	3.4793
	60	3.3798	3.3798	3.3799
	90	3.2425	3.2426	3.2425
3^{rd}				
	30	11.1691	11.1691	11.1693
	60	11.6044	11.6040	11.6046
	90	12.2646	12.2644	12.2649
4^{th}				
	30	21.4475	21.4470	21.4489
	60	20.1533	20.1531	20.1545
	90	18.7295	18.7301	18.7307

These four lowest non-dimensional frequencies correspond to bending modes as: ω_{1z}, ω_{1y}, ω_{2z} and ω_{2y}, respectively. Due to the pretwist, exciting the beam with either of these modes called driven mode will induce a compagnon mode in the transverse direction. In Fig. 5, the mode shapes of these frequencies with their compagnion modes corresponding to $\alpha = 30^o$ are shown. It can be seen that the compagnion modes are of the same order of the excited ones. Furthermore, these modes are not coupled with the stretching and torsion modes, which explain the accordance between results given in Table 2.

Fig. 2 shows the response curve of a fixed-free isotropic beam under a concentrated harmonic excitation at the tip, with dimensionless frequencies on the horizontal axis. The beam used here is the one treated in [31] for the modeling of an articulated rotor blades. The

Table 1
Comparison of the first two non-dimensional natural frequencies of rotating beam . Case of Timoshenko beam, except for the first line where EB stands for an Euler beam ($\delta_h = 0,\ k_sG/E = 0.25$)

β	$\Omega^* = 0$			$\Omega^* = 4$			$\Omega^* = 8$		
	Present	[6]	[7]	Present	[6]	[7]	Present	[6]	[7]
EB	3.5160	3.5160	3.5059	5.5850	5.5850	5.5850	9.2568	9.2568	9.2568
	22.0345	22.0345	22.0296	24.2733	24.2733	24.2726	29.9954	29.9954	29.9950
50	3.4998	3.4998	3.5000	5.5564	5.5616	5.5623	9.1947	9.2096	9.2132
	21.3547	21.3547	21.3692	23.5630	23.6061	23.6240	29.1908	29.3215	29.3501
25	3.4527	3.4527	3.4534	5.4730	5.4951	5.4980	9.0113	9.0854	9.0975
	19.6497	19.6497	19.6965	21.5680	21.9557	22.0126	27.3632	27.7082	27.7933
16.67	3.3787	3.3787	3.3803	5.3408	5.3954	5.4013	8.7107	8.9209	8.9423
	17.547	17.547	17.6251	19.6555	19.9662	20.0593	24.8949	25.8362	25.9651
12.5	3.2837	3.2837	3.2863	5.1680	5.2749	5.2840	8.2793	8.7456	8.7746
	15.4883	15.4883	15.5873	17.5032	18.0628	18.1781	22.4037	24.0479	24.1961
10	3.1738	3.1738	3.1774	4.9635	5.1448	5.1570	7.8468	8.5735	8.6077
	13.6607	13.6607	13.7694	15.6020	16.3946	16.5184	20.8700	22.3506	22.4979

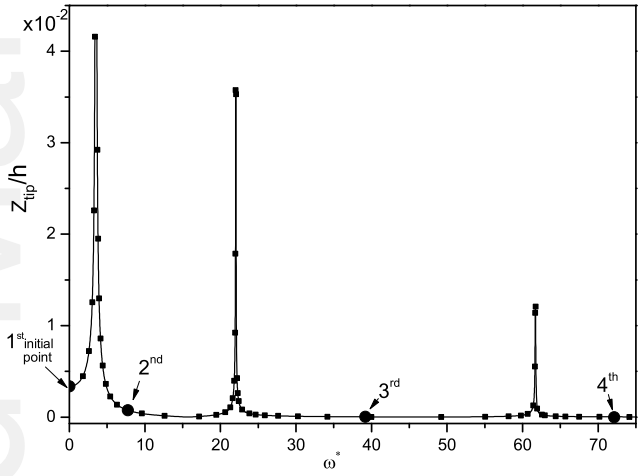

Fig. 2 Response curve of fixed-free isotropic and prismatic beam excited harmonically at the tip. ($F_0 = 10^{-3}N,\ L = 10\ m$) – This curve is obtained by three steps using a Padé continuation version of ANM. (• series, and ▪ Padé)

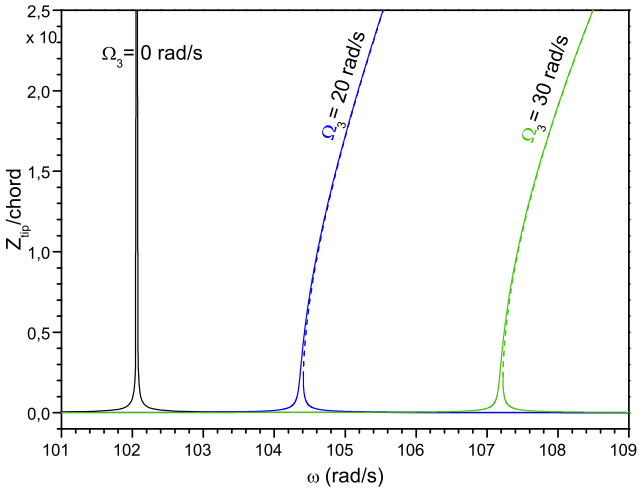

Fig. 3 Response curve of fixed-free isotropic and prismatic beam excited harmonically at the tip. ($F_0 = 10^2N,\ L = 10m$) – angular speed effect

numerical values are: $A = 0.2 \times 0.1 = 0.02\ m^2,\ E = 1.792\ 10^{13}N/m^2, \nu = 0.3,\ \rho = 1770\ kg/m^3,\ L = 1\ m.$ Three modes are obtained by four initial points; i.e. three steps, using a Padé continuation version of ANM. The same result is obtained by series version of ANM and the PAL method but with four discontinuous segments. Those frequency values correspond to Euler-Bernoulli beam with zero angular speed presented in Table 1.

Fig. 3 shows the angular speed effect on the response curves of a beam harmonically excited at the tip. It can be observed that the natural frequency, which represents the first flap bending mode, increases with the increase of the angular speed and the response curve becomes nonlinear. Fig. 4 shows that this nonlinearity depends on the angular speed's value, and the beam exhibits hardening behavior. It is mentioned in [37] that a rotating beam may exhibit hardening or softening behavior depending on the geometrical and kinematical conditions.

We focus now on the effects of the parameters: the hub radius and the pretwist on the linear frequencies. Even for these parameters changed, the nonlinearity is still low and has not been influenced. Fig. 6 illustrates the influence of the hub radius and the pre-twist applied on the dynamic characteristics of the same beam with angular speed. It can be observed, that the response

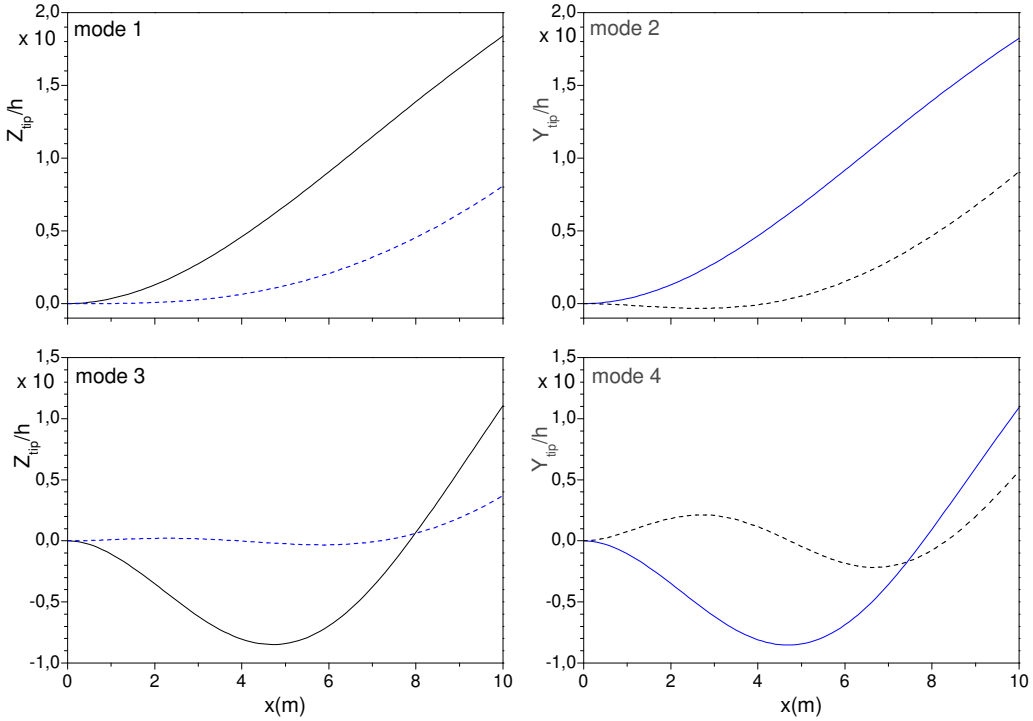

Fig. 5 First four mode shapes with their compagnon modes, $\alpha = 30^0$ and $L = 10\ m$, continued line (—): driven mode, dashed line (---): compagnon mode on the tranversal direction

curve moves to the right and the natural frequency increases with these parameters.

Thus, for isotropic prismatic beams having a diagonal stiffness and mass matrices, the principal cause of nonlinearity is the angular speed. The nonlinear term in Eq. (21) i.e. $\bar{C}$ matrix desappears in zero angular speed case.

3.2 Composite beam

The model of composite beam used in this study is the Active Twist Rotor (ATR) blade presented in [15, 27, 32]. This blade was developed for an articulated rotor, it is made from E-glass, S-glass and Active Fiber Composite (AFC) with an airfoil section NACA 0012 as illustrated in Fig. 7, and a span $L = 1.397m$. Details of the ATR blade can be found in [27,32] and the structure parameters are given in Table 4. These parameters are determined using the area centroid of the cross-section as the reference line, the axis x_2 and x_3 are principal, i.e. $i_{23} = 0$ and the mass centroid is localized at ($\bar{x}_2 = -6.9240 \times 10^{-4}\ m, \bar{x}_3 = 0\ m$). In these previous papers [15, 27, 32], only the angular speed effect on the linear frequencies is reached. Here we study the nonlinearity of the response curve for this hingeless blade. For generality and simplicity, the actuation forces characterized with their coupling forces-moments are not considered.

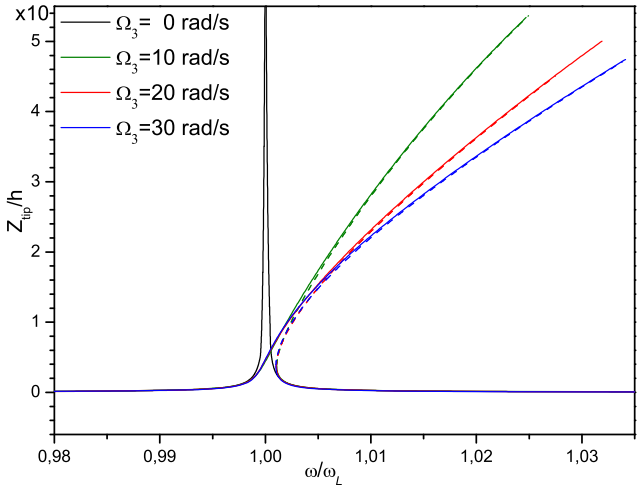

Fig. 4 Response curve of fixed-free rotating isotropic and prismatic beam excited harmonically at the tip ($F_0 = 5 \cdot 10^2\ N,\ \Omega_3 = 0 \div 30\ rad/s$, --- unstable solution)

Table 3 presents the first four natural frequencies (bending modes) with and without the angular speed.

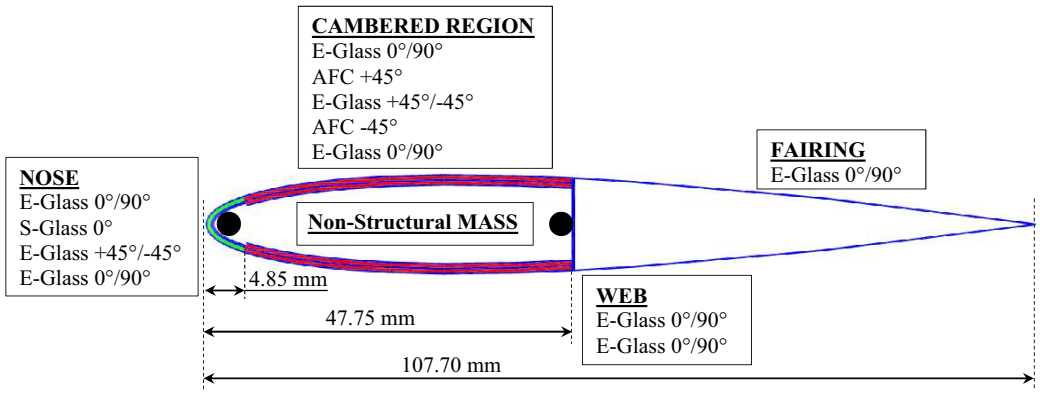

Fig. 7 Profile of the ATR blade and Ply-up [27]

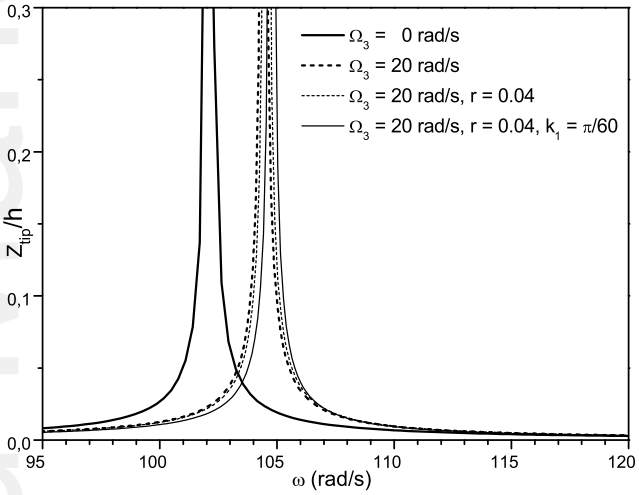

Fig. 6 Response curve of fixed-free isotropic and prismatic beam excited harmonically at the tip. ($F_0 = 10^2 N,\ L = 10m$) – hub radius and pretwist angle effects

It can be observed that all modes increase with increasing angular speed and for these cases $\omega_{2/z} \approx \omega_{1/z} + \omega_{1/y}$, which is defined as an internal resonance which involves more than two frequencies of flexural-flexural type [28, 38, 39, 41]. This phenomenon desappears for angular speed $\Omega_3 > 20\ rad/s$. In [38],the interaction between these modes and the exchange of energy are discussed in both cases, with and without angular speed.

Fig. 8 shows the response curve, obtained with two methods of continuation; the ANM and the PAL continuation methods. It represents the first flapwise bending mode, where the magnitude of concentrated harmonic excitation applied at the tip is $F_0 = 20N$ with zero angular speed $\Omega_3 = 0\ rad/s$. It can be observed that the nonlinearity is more noticeable for this anisotropic

Table 3
The lowest four natural frequencies of the ATR, for a static and rotating cases

Mode	$\Omega_3 = 0 rad/s$		$\Omega_3 = 10 rad/s$	$\Omega_3 = 20 rad/s$
	[15]	Present	Present	Present
$1^{st}/z$	13.68	13.64	17.44	25.53
$1^{st}/y$	70.76	70.60	70.73	71.10
$2^{nd}/z$	86.71	84.40	88.13	98.47
$3^{rd}/z$	248.8	232.0	235.5	246.5

beam and the perfect coherence between both methods of continuation. The stability is studied by using the method presented in section 2.7, the unstable solutions are presented by the dashed lines. Although there is no damping introduced in either the mathematical model nor in the numerical procedures, the curve has a damping behavior, this is due to internal resonance between the in-plane and out-of-plane displacements, which makes apparent the gyroscopic effect, and thus the pseudo-damping phenomenon [40]. This explains, the natural frequency shift in downward when the force amplitude is increased, as it is shown in Fig. 11

Fig. 9(a, b), show the accuracy evaluation of these two methods of continuation around the first mode ($0 \leqslant \omega \leqslant 25\ rad/s$), the residual is obtained from the norm of the vector $\mathcal{F}(\bar{q}, \omega)$ Eq. (21) and based on the parameters of convergence fixed above. The truncation order is taken $n = 15$ in Fig. 9a, and $n = 20$ in Fig. 9b. It can be observed that the PAL is more accurate than the ANM in spite of increasing the order of truncation, but as it is depicted in Table 4, the ANM is generally less expensive in CPU time than PAL for the lower values of tolerance ($\eta_s = 10^{-7}$).). This is mainly due to the number of the Jacobian matrix inversion, which is

Table 4
Structure parameters of the ATR blade [15, 22]

$L = 1.3970\ \ m$	$\mu = 6.9310 \times 10^{-1}\ \ kgm^{-1}$	
$\bar{x}_2 = -6.9240 \times 10^{-4}\ m$	$\bar{x}_3 = 0.\ \ m$	
$\mathbb{i}_2 = 6.4630 \times 10^{-6}\ \ kgm$	$\mathbb{i}_3 = 3.7018 \times 10^{-4}\ \ kgm$	$\mathbb{i}_{23} = 0.\ \ kgm$
$\mathbb{U} = \begin{bmatrix} \mathbb{U}_{11} & 0 & 0 \\ 0 & \mathbb{U}_{22} & 0 \\ 0 & 0 & \mathbb{U}_{33} \end{bmatrix}$	$\mathbb{V} = \begin{bmatrix} 0 & 0 & \mathbb{V}_{13} \\ 0 & 0 & 0 \\ \mathbb{V}_{31} & 0 & 0 \end{bmatrix}$	$\mathbb{W} = \begin{bmatrix} \mathbb{W}_{11} & 0 & 0 \\ 0 & \mathbb{W}_{22} & 0 \\ 0 & 0 & \mathbb{W}_{33} \end{bmatrix}$
$\mathbb{U}_{11} = 1.6377 \times 10^{6}\ \ N$	$\mathbb{U}_{22} = 2.0300 \times 10^{5}\ \ N$	$\mathbb{U}_{33} = 2.3150 \times 10^{4}\ \ N$
$\mathbb{V}_{13} = -9.7975 \times 10^{3}\ Nm$	$\mathbb{V}_{31} = -1.4820 \times 10^{2}\ Nm$	
$\mathbb{W}_{11} = 3.5330 \times 10^{1}\ Nm^2$	$\mathbb{W}_{22} = 3.9868 \times 10^{1}\ Nm^2$	$\mathbb{W}_{33} = 1.1381 \times 10^{3}\ Nm^2$

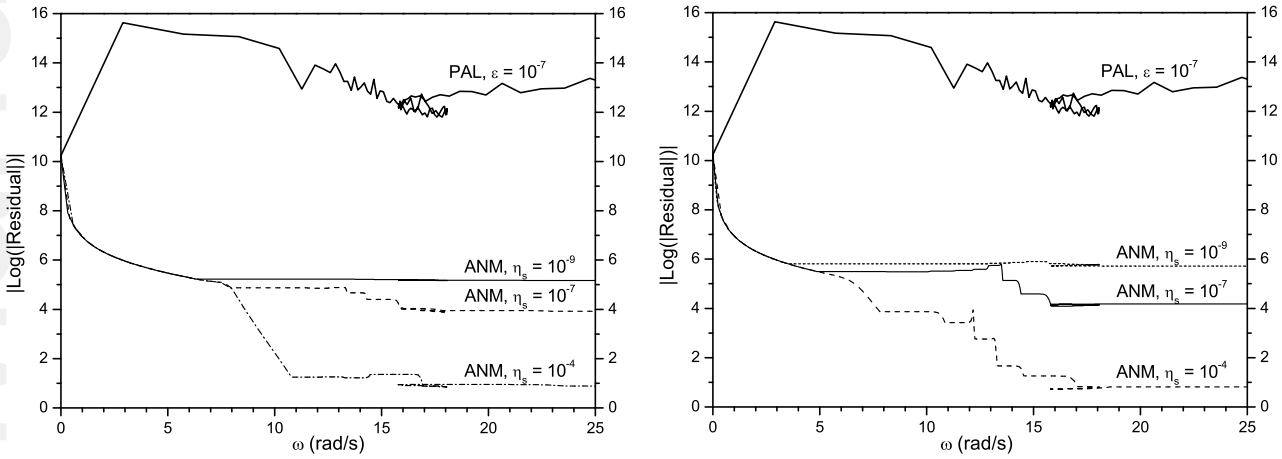

(a) Truncation order $n = 15$ **(b)** Truncation order $n = 20$

Fig. 9 Accuracy of ANM series-continuation VS. PAL (Case of ATR blade excited harmonically at the tip, $F_0 = 20N$ and $\Omega_3 = 0\ rad/s$)

lower with ANM than with PAL. Another advantage of using ANM lies in the analytic form of the solutions due to the polynomial approximations or Padé approximants, and the step which is automatically adjusted and adapted to the difficulty of the branch, instead of the point by point solution obtained with the iterative method PAL, with a step (Δs) Eq.(40).

Furthermore, Table 5 shows that the computational time increases with the order of truncation, whereas the number of steps (i.e. the number of matrix inversions) decreases. This is due to the time to build the right-hand-side D_p Eq. (31) which is greater, for the considered number of unknowns $\bar{q}_i$, than the time to inverse the Jacobian matrix. In classical ANM applications, where the spatial discretization is realized with the finite element method, the longest amount of CPU time is spent in the triangulation of the Jacobian matrix when the number of unknowns is significant.

Fig. 11 shows the excitation magnitude effect for non-rotating blade. For this case, the response curve of the free vibration bifurcates from the point ($\bar{q} = 0, \omega_1 = 13.64\ rad/s$). If an angular speed is applied, another point of bifurcation can be defined by ($\omega > \omega_1,\ \bar{q} \neq 0$), corresponding to steady state equilibrium. It can be observed that the maximum amplitude of these response curves is insensitive to the excitation strength, which is directly related to the existence of the internal resonance [39], defined as saturation phenomenon which occurs in the forced response of a dynamical system with quadratic nonlinearities in presence of internal resonance [29]. Fig.10 shows these two transverse displacements, the driven mode is along z and the compagnion mode is along y. It can be seen that there no tongue or secondary branches and thus the compagnion mode curve is due to both coupling and internal resonnance. Fig. 12 illustrates the new shape of the response curve caused by a non-zero angular speed $\Omega_3 = 20\ rad/s$, obtained by the two versions of ANM series/Padé and by

Table 5
Step number, CPU times and residual for $\omega = [0,\ 25]\ rad/s$. Case of ATR blade excited harmonically at the tip, ($F_0 = 20N$ and $\Omega_3 = 0\ rad/s$)

	Asyptotic Numerical Method (ANM - series)						Pseudo-arclength
	Truncation order n=15			Truncation order n=20			PAL
Tolerance	$\eta_s = 10^{-4}$	$\eta_s = 10^{-7}$	$\eta_s = 10^{-9}$	$\eta_s = 10^{-4}$	$\eta_s = 10^{-7}$	$\eta_s = 10^{-9}$	$\epsilon = 10^{-7}$
Step number	14	24	34	13	19	24	284
CPU time (s)	117	198	288	185	271	340	224
|Log10(Residual)| at $\omega = 25 rad/s$	0.815	3.92	5.17	0.89	4.18	5.72	13.22

Table 6
Step number, CPU times and residual for $\omega = [0,\ 30]\ rad/s$. Case of ATR blade excited harmonically at the tip, ($F_0 = 20N$ and $\Omega_3 = 20\ rad/s$)

	Asyptotic Numerical Method (ANM - series)						Pseudo-arclength
	Truncation order n=15			Truncation order n=20			PAL
Tolerance	$\eta_s = 10^{-4}$	$\eta_s = 10^{-7}$	$\eta_s = 10^{-9}$	$\eta_s = 10^{-4}$	$\eta_s = 10^{-7}$	$\eta_s = 10^{-9}$	$\epsilon = 10^{-7}$
Step number	25	45	63	20	34	45	837
CPU time (s)	217	387	540	310	473	624	671
|Log10(Residual)| at $\omega = 30\ rad/s$	3.25	0.46	0.57	3.90	0.76	0.88	9.22

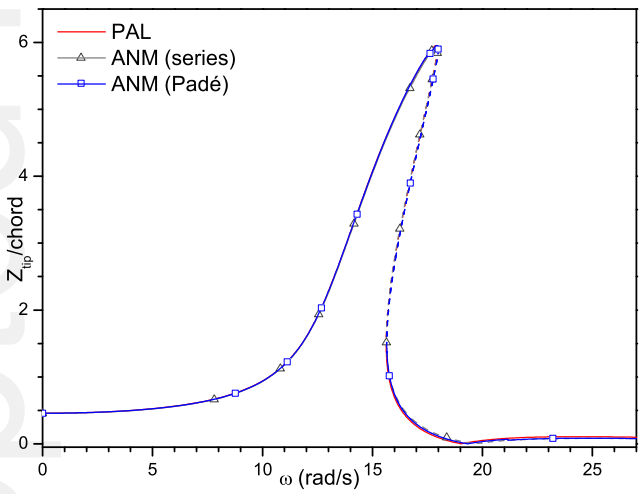

Fig. 8 Response curve of ATR blade excited harmonically at the tip. ($F_0 = 20N,\ \Omega_3 = 0\ rad/s$) Point symbols indicate the initial points of ANMs; △ series, and ▫ Padé. Dashed zone: unstable sloution

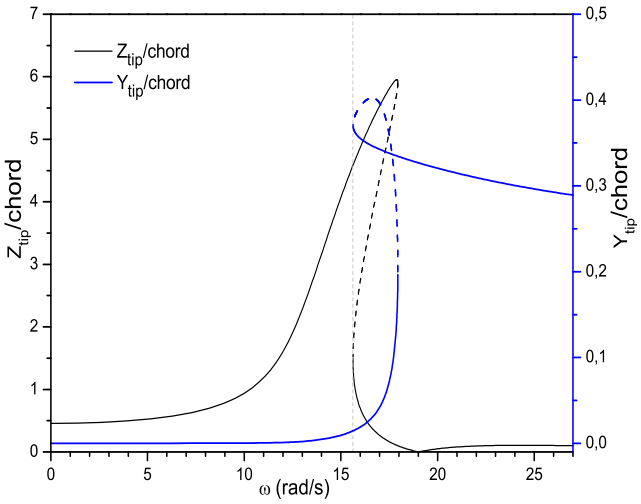

Fig. 10 In-plane and out-off-plane response curves of ATR blade excited harmonically at the tip. ($F_0 = 20N,\ \Omega_3 = 0\ rad/s$). Dashed zone: unstable sloution

PAL. The frequency of the first mode increases from 13.64 to 25.53 rad/s as it is presented in Table 3. The jump at ($\omega \approx 19\ rad/s$) is due to an intermittent exchange of energy; As it is explained in [38, 39], when the beam is excited at the vicinity of the out-of-plane mode $\omega_{1/z}$ in the presence of such internal resonance, there will be an interaction and an exchange of energy with the in-plane mode $\omega_{1/y}$.

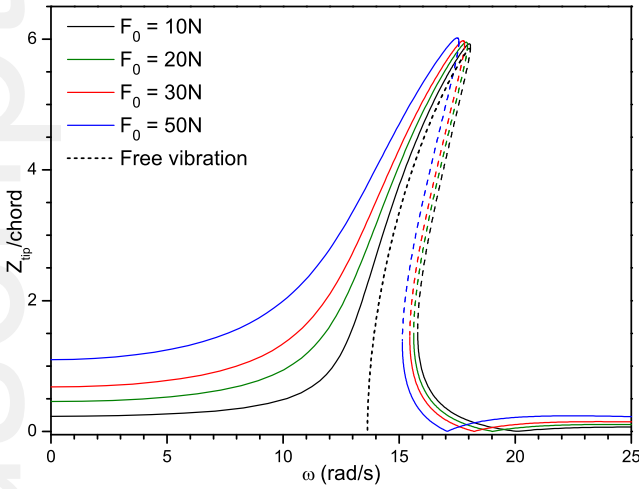

Fig. 11 Response curves of ATR blade excited harmonically at the tip– Force amplitude effect ($F_0 = 10N,\ 20N\ , 30N$ with $\Omega_3 = 0\ rad/s$)

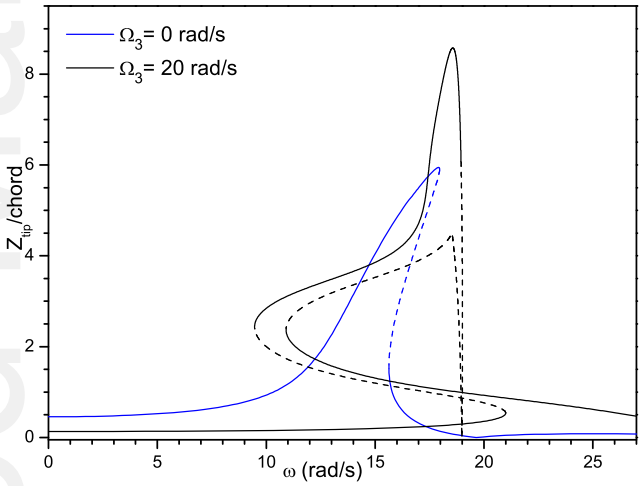

Fig. 12 Response curve of ATR blade excited harmonically at the tip– Angular speed effect ($F_0 = 20N$, and $\Omega_3 = 20\ rad/s$), △ and ▪ are the initial point of ANM(series)

The new response curve has an unstable zone that begins from the first turning point, from when a jump can happen and the amplitude of resonance is less than in the dotted response curve, with zero angular speed, which provides some kind of dumping to the blade. One can also observe the decrease in the response of the static state i.e. the initial point of the curve. A singular point is also observed at $\omega = 18.986\ rad/s$, which cannot be reached because of jumps at turning points.

In terms of convergence, as is shown in Table 6, the best final residual for the ANM (series) is obtained with tolerance $\eta_s = 10^{-4}$. The PAL method of continuation

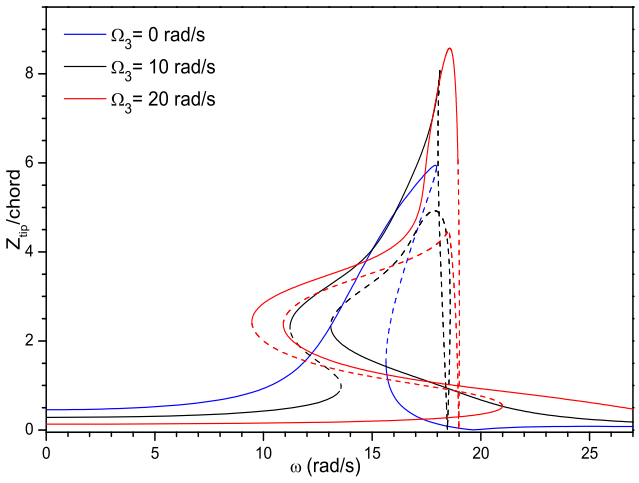

Fig. 13 Response curve of ATR blade excited harmonically at the tip.($F_0 = 20N$) – Different values of the angular speed

is more accurate, with maximum of 3 to 4 iterations in the correction part of calculus.

The loss of ANM's accuracy, detected even for higher order of truncation, has also been observed in the framework of vibrations of plates [33]. It can be improved by introducing a correction in the ANM calculations, such methods proposed in [34] which have the advantage of improving the quality of the ANM solution, without increasing the CPU times.

Fig. 13 illustrates the response curves of this blade for two values of angular speed; 10 and 20 rad/s. The natural frequency changes but the general behavior of the curves is the same. This behavior, which has even been observed even for other angular speed values, leads us to conclude that angular speed transform the system from hard to soft.

4 Conclusion

In this paper, dynamic nonlinearities of a composite beam subjected to harmonic excitations are treated. The mathematical model is based on the intrinsic equations for the dynamic of beams undergoing small strains and large global deformations. The asymptotic numerical methods with series-continuation, Padé continuation and the pseudo-arclength continuation method are elaborated for numerical solutions. Hence, algorithms for those two continuation methods have been developed. For both ANM techniques, the final nonlinear solution is obtained by solving a sequence of linear systems having the same matrix to be inverted. A compar-

ative study dealing with composite blade shows that, as far as the optimal computational parameters is concerned, the pseudo-arclength continuation method is expensive, but more accurate. Firstly, numerical experiments are conducted on homogenous isotropic beams. Natural frequencies for various values of angular speed, hub radius and pretwist angles are obtained. Compared with those of the literature, the obtained results are in good agreement for Euler-Bernoulli beam and Timoshenko beam with zero angular speed. They deviate considerably for the case of Timoshenko beam with nonzero angular speed. This is explained by the fact that the gyroscopic coupling terms are not neglected in this approach. Continuation methods are tested for response curves of isotropic prismatic beams revealing a weak nonlinearity resulting from the presence of the angular speed. Secondly, composite beams are analyzed. Both continuation methods show the presence of nonlinearities. The results show that the response curves become distorted and complexe by increasing the angular speed, especially with the presence of an internal resonance

The present study only deals with the fixed-free beams with moderate angular speeds. The obtained results are not relative to the evaluation of the frequencies (i.e., eigenvalues), but also analyzed nonlinearities through response curves, which is a crucial subject. Present approach can be extended for other types of structures with different geometrical and dynamical conditions.

Acknowledgment

The authors are grateful for the encouragement and useful comments of two anonymous reviewers.

References

1. Southwell, R., Gough, F.: The transverse vibration of airscrew blades. British A. R. C. Reports and Memoranda **766** (1921)
2. Putter, S., Manor, H.: Natural frequencies of radial rotating beams. J. Sound Vib. **56**, 175–85 (1978)
3. Wright, A., Smith, C., Thresher, R., Wang, J.: Vibration modes of centrifugally stiffened beams. J. App. Mech. **49**, 197–202 (1982)
4. Klein, L.: Transverse vibrations of non-uniform beam. J. Sound Vib. **37**, 491–505 (1974)
5. Swaminathan, M., Rao, J.: Vibrations of rotating pretwisted and tapered blades. Mech. Mach. Theory **12**, 331–337 (1977)
6. Ozdemir, O.O., Kaya, M.O.: Flapwise bending vibration analysis of rotating double-tapered timoshenko beam. Arch. Appl. Mech. **78**, 379–392 (2008)
7. Zhu, T.L.: Free flapwise vibration analysis of rotating double-tapered timoshenko beams. Arch. Appl. Mech. **82**, 479–249 (2012)
8. Yoo, H.H., Shin, S.H.: Vibration analysis of rotating cantilever beams. J. Sound Vib. **212**, 807–828 (1998)
9. Yoo, H.H., Park, J.H., Park, J.: Vibration analysis of rotating pre-twisted blades. Comput. Struct. **79**, 1811–1819 (2001)
10. Borri, M., Mantegazza, P.: Some contributions on structural and dynamic modeling of helicopter rotor blades. l'aerotecnica Missili e Spazio **64**, 143–154 (1985)
11. Bauchau, O.A., Kang, N.K.: A multibody formulation for helicopter structural dynamic analysis. J. Am. Helicopter Soc. **38**, 3–14 (1993)
12. Hodges, D.H.: A mixed variational formulation based on exact intrinsic equations for dynamics of moving beams. Int. J. Solids Struct. **26**, 1253–1273 (1990)
13. Hodges, D.H.: Geometrically exact, intrinsic theory for dynamics of curved and twisted anisotropic beams. AIAA **41**, 1131–1137 (2003)
14. Patil, M.J., Althoff, M.: Energy-consistent, galerkin approach for the nonlinear dynamics of beams using intrinsic equations. J. Vib. and Control **17**, 1748–1758 (2010)
15. Althoff, M., Patil, M.J., Traugott, J.P.: Nonlinear modeling and control design of active helicopter blades. In proceeding of the 14th adaptive structures conference. Newport, Rhode Island, AIAA-2006-2040 (2006)
16. Althoff, M., Patil, M.J., Traugott, J.P.: Nonlinear modeling and control design of active helicopter blades. J. Am. Helicopter Soc. **57**, 1–11 (2012)
17. Elhage-Hussein, A., Potier-Ferry, M., Damil, N.: A numerical continuation method based on padé approximants. Int. J. Solids Struct. **37**, 6981–7001 (2000)
18. Cochelin, B., Damil, N., Potier-Ferry, M.: Asymptotic numerical methods and padé approximants for non-linear elastic structures. Int. J. Numer. Method. Eng. **37**, 187–213 (1994)
19. Azrar, L., Boutyour, E.H., Potier-Ferry, M.: Non-linear forced vibrations of plates by an asymptotic-numerical method. J. sound Vib. **252**, 657–674 (2002)
20. Abdoun, F., Azrar, L., Daya, E.M., Potier-Ferry, M.: Forced harmonic response of viscoelastic structures by an asymptotic numerical method. Comput. Struct. **87**, 91–100 (2009)
21. Boumediene, F., Miloudi, A., Cadou, J.M., Duigou, L., Boutyour, E.H.: Nonlinear forced vibration of damped plates by an asymptotic numerical method. Comput. Struct. **87**, 1508–1515 (2009)
22. Guevel, Y., Boutyour, E.H., Cadou, J.M.: Automatic detection and branch switching methods for steady bifurcation in fluid mechanics. J. Comp. Physics **230**, 3614–3629 (2011)
23. Pérignon, F.: Vibrations forcées de structures, élastiques; non-linéaire. Ph.D. thesis, Université Aix-Marseille II (2004)
24. Yu, W., Hodges, D.H., Volovoi, V., Cesnik, C.E.S.: On timoshenko-like modeling of initially curved and twisted composite beams. Int. J. Solids Struct. **39**, 5101–5121 (2002)
25. Hodges, D.H.: Nonlinear composite beam theory. AIAA, Reston VA (2006)
26. Abramowitz, M., Stegun, I.A.: Handbook of mathematical functions. Dover, New York, NY (1968)
27. Trogott, J.P., Patil, M.J., Holzapfl, F.: Nonlinear modeling of integrally actuated beams. Aerosp. Sci. Technol. **10**, 509–518 (2006)

28. Neyfeh, A.H., Balachandran, B.: Applied nonlinear dynamics analytical, computational and experimental methods, pp. 423-459. Wiley-VCH (2004)
29. Neyfeh, A.H., Mook, D. T.: Nonlinear oscillations. Wiley-Inc (1995)
30. Zhu, T.L.: The vibrations of pre-twisted rotating timoshenko beams by rayleigh-ritz method. Arch. Appl. Mech. **47**, 395–408 (2011)
31. Ghorashi, M.: Nonlinear analysis of the dynamics of articulated composite rotor blades. Nonlinear Dynam. **67**, 227–249 (2012)
32. Shin, S., Cesnik, C.E.S.: Integral twist actuation of helicopter rotor blades for vibration reduction. NASA, Techdoc 20010110792 (2001)
33. Boumediene, F., Duigou, L., Boutyour, E.H., Miloudi, A., Cadou, J.M.: Nonlinear forced vibration of damped plates coupling asymptotic numerical method and reduction models. Comput. Mech. **47**, 359–377 (2011)
34. Cadou, J.M., Duigou, L., Damil, N., Potier-Ferry, M.: Convergence acceleration of iterative algorithms. applications to thin shell analysis and navier–stokes equations. Comput. Mech. **43**, 253–264 (2008)
35. Stoykov, S., Ribeiro, P.: Stability of nonlinear periodic vibrations of 3D beams. Nonlinear Dynam. **66**, 335–353 (2011)
36. Lazarus, A., Thomas, O.: A harmonic-based method for computing the stability of periodic solutions of dynamical systems. C. R. Méc. **338**, 510–517 (2010)
37. Turhan, O., Bulut, G.: On nonlinear vibrations of a rotating beam. J. sound Vib. **322**, 314–335 (2009)
38. Bekhoucha, F., Rechak, S., Duigou, L., Cadou, J.M.: Nonlinear forced vibrations of rotating composite beams with internal combination resonance. In Proceeding of the fifth international conference on design and modeling of mechanical systems, CMSM 2013, Tunisia, March 25-27, 2013. Springer, 159–166 (2013)
39. Zaretzky, C.L., Crespo Da Silva, M.R.M.: Nonlinear flexural-flexural-torsional interactions in beams including the effect of torsional dynamics.II: combination resonance. Nonlinear Dynam. **5**, 161-180 (1994)
40. Combescure, D., Lazarus, A.: Refined finite element modelling for the vibration analysis of large rotating machines: Application to the gas turbine modular helium reactor power conversion unit. J. sound Vib. **318**, 1262–1280 (2008)
41. Vakakis, A., F.: Fundamental and Subharmonic Resonances in a System with a '1-1' Internal Resonance. Nonlinear Dynam. **3**, 123–143 (1992)